Manuscript prepared for Atmos. Chem. Phys. Discuss.
with version 2.2 of the LaTeX class copernicus_discussions.cls.
Date: 20 March 2015

Meridionally-Tilted Ice Cloud Structures in the Tropical Upper Troposphere as Seen by CloudSat

J. Gong[1,2], D. L. Wu[2], and V. Limpasuvan[3]

[1]University Space Research Association, Columbia, MD, USA
[2]Climate and Radiation Branch, MC 613.2, NASA/Goddard Space Flight Center, Greenbelt, MD, USA
[3]School of Coastal and Marine Systems Science, Coastal Carolina University, Conway, SC

Correspondence to: J. Gong (jie.gong@nasa.gov)

Abstract

It remains challenging to quantify global cloud properties and uncertainties associated with their impacts on climate change because of our poor understanding of cloud three-dimensional (3D) structures from observations and unrealistic/unconsidered characterization of 3D cloud effects in Global Climate Models (GCMs). In this study we find cloud 3D effects can cause significant error in cloud ice and radiation measurements if it is not taken into account appropriately.

One of the cloud 3D complexities, the slantwise tilt structure, has not received much attention in research and even less report is given on its global perspective. A novel approach is presented here to analyze the ice cloud water content (IWC) profiles retrieved from CloudSat and a joint radar-lidar product (DARDAR). By integrating IWC along different tilt angles, we find that upper-troposphere (UT) ice cloud mass between 11 and 17 km is tilted poleward from active convection centers in the tropics ($[30^{\circ}S,\ 30^{\circ}N]$). This systematic tilt in cloud mass structure is expected from the mass conservation principle of the Hadley circulation with the divergent flow of each individual convection/convective system from down below, and its existence is further confirmed from cloud-resolving scale Weather Research and Forecasting (WRF) model simulations. Thus, additive effects of tilted cloud structures can introduce $5-20\%$ variability by nature or bring an error to satellite cloud/hydrometeor ice retrievals if simply converting it from slant to nadir column. A surprising finding is the equatorward tilt in middle tropospheric (5-11 km) ice clouds, which is also evident in high-resolution model simulations but not in coarse-resolution simulations with cumulus parameterization. The observed cloud tilt structures are intrinsic properties of tropical clouds, producing synoptic distributions around the ITCZ. These findings imply that current interpretations based on over-simplified cloud vertical structures could lead to substantial cloud measurement errors and induce subsequent impact on understanding cloud radiative, dynamical and hydrological properties.

1 Introduction

Understanding and predicting climate changes requires accurate measurements of Earths radiation budget. Due to its large variability in space and time, cloud radiative effect (CRE) poses arguably the greatest difficulty in estimating the radiation budget balance at both top of atmosphere (TOA) and surface. Complexities in cloud three-dimensional (3D) structures, in particular, are one of the primary sources of the uncertainty and difficulty, which affect satellite cloud observations as well as CRE calculations in Global Climate Models (GCMs).

Cloud 3D effects manifest themselves as multiple forms: the bulk outlook is visibly irregular, and the internal mass structures are also inhomogeneous. The detailed cloud vertical structures are difficult to be resolved in passive satellite observations. Subsequently, they are either neglected or significantly simplified in GCMs. Oversimplified or improper treatment of the cloud 3D structure increases the uncertainties or generates additional biases of satellite cloud property retrievals [Marshak et al., 2006], GCM simulations of cloud fields [Cahalan et al. (1994)] and atmospheric constituent retrievals [Ming and Zhang (2014)].

As one key vertical aspect of cloud 3D structure, cloud slantwise tilt is inherently linked to cloud thermodynamics and gravity waves coupled with heating profiles. Systematic cloud tilt structures can have profound impacts on cloud remote sensing and radiation calculations. For example, they partially account for the anisotropy of the cloud radiative forcing [Fu et al. (2000); Gong and Wu (2013)] and modulate the hydrological cycle [Naud et al. (2010)]. Neglecting or misrepresenting of the cloud tilt induces additional biases in satellite retrieval of cloud properties [e.g., Hong et al. (2005)] and increases uncertainty of model CRE estimation [e.g., Li and Barker (2002)]. In GCM, cloud slantwise tilt is tied to the overlap parameter, which is assumed to be maximum-random globally in most GCMs to achieve the desired cloud fraction or radiation balance. However, studies have shown that this parameter has large geographical and temporal variations around the globe [Oreopoulos et al. (2012); Yuan and Oreopoulos (2013)], which implied that the prevailing assumption in GCMs needed to be improved and could be constrained by satellite observations.

Very few global surveys are reported on cloud tilt structures so far. It is difficult for passive

sensors because of their coarse vertical/horizontal resolutions and variable penetration depths, yielding ambiguous information about cloud internal structures. Nevertheless, Gong and Wu [2011; 2013a, b] were able to derive cloud tilt statistics of the upper troposphere cloud in the zonal direction using radiance data from NASAs Aqua Atmospheric Infrared Sounder (AIRS) and NOAAs Microwave Humidity Sounder (MHS). Ground-based cloud radars often observe tilt structures locally but in time domain and are sometimes contaminated by rain signals [Huang et al. (2012)].

In this study we make a novel use of polar-orbiting CloudSat Cloud Profiling Radar (CPR) data to characterize global cloud tilt structures in the meridional direction. CloudSat provides an unprecedented quality of high-resolution ice water content (IWC) measurements for investigating cloud internal structures in the upper-troposphere (UT) [Protat et al. (2009)]. By integrating CloudSat IWC along different slant paths, we find that ice clouds at height greater than 11 km are systematically tilted poleward from active convection centers in the tropics [$30^\circ S$, $30^\circ N$]. The observed cloud tilt structures resemble the divergent flow at the top of deep convection and convergence below in the tropical branch of the Hadley circulation.

2 Datasets, model and methodology

Launched in April 2006 into a Sun synchronous orbit, CloudSat has the same equator crossing time (∼1:30 pm/am local time) on the ascending/descending as other A-Train constellation members. CloudSat CPR, a 94 GHz nadir-scan radar, returns the aggregation of 600 pulses every 0.16 sec during which the platform travels 1.1 km[1]. The CloudSat IWC product from 2B-CWC-RO V008 has a vertical resolution of $\sim$ 0.25 km and horizontal resolution of $\sim$ 1.1 km. Despite having been validated against aircraft measurements and many other independent observations [Protat et al. (2009); Wu et al. (2009)], the CloudSat IWC product still has some known issues. Thin cirrus is normally below its detection threshold, and the W-band radar tends to suffer from attenuation and/or multiple-scattering below 9 km when cloud is heavily precipitating [Protat et al. (2009)]. Moreover, the current IWC product has an estimated uncertainty

[1] http://disc.sci.gsfc.nasa.gov/atdd/documentation/ATrainTracks.pdf

of up to $\sim 40\%$ [Austin et al. (2009)]. CALIPSOs Cloud-Aerosol Lidar with Orthogonal Polarization (CALIOP) is a great complement to fill in the thin ice cloud part of the picture missed by CloudSat. A recently published joint IWC retrieval product (DARDAR) combining CloudSat-CALIPSO-MODIS (Moderate Resolution Imaging Spectroradiometer) observations shows robust consistency with CloudSat IWC without losing the signal from thin ice clouds [Delanoe et al. (2010); Delanoe et al. (2013); Eliasson et al. (2013)]. Due to the limitation of the CloudSat IWC product, this study will focus primarily on ice cloud above 9 km. Nonetheless, we will briefly address the tilt characteristic of ice cloud between 5 km (roughly the freezing height) and 9 km as cloud tilt structure continuously evolve with height.

Fig. 1a and 1b show two examples of CloudSat IWC curtains at two random days, when one can see anvils and cirrus clouds associated with a tropical deep convection fanning out meridionally in the upper troposphere (Fig. 1a), while the clouds in the mid-latitude frontal system case apparently all tilt northward (Fig. 1b). DARDAR data (Fig. 2) are broadly consistent with those from CloudSat with some subtle differences. For example, DARDAR ice cloud product reveals a thin cirrus layer above the anvil clouds in the tropical deep convection case that is not detected by CloudSat.

To better understand the genesis of cloud tilt structures, we carried out mesoscale numerical simulations using Weather Research and Forecasting (WRF) model in a tropical region. As a regional mesoscale model, WRF has been widely used for regional weather/climate studies and includes sophisticated cloud microphysics to represent the real atmosphere as well as possible [2]. Yet, it is able to simulate the atmosphere for a much larger domain than cloud resolving models (CRMs). For the purpose of the current study, WRF simulations are designed to have horizontal grid box (ΔL) of 3.3 km and vertical resolution (ΔZ) of $\sim$ 0.5 km with cumulus parameterization turned off. As a result, WRF is used as a cloud-resolving model in a sense. The specific settings and simulation designs will be discussed in the next section.

In the CloudSat data analysis, we introduce a new approach for integrating the IWC measured along the orbital curtain [like that shown in Fig. 1]. To mimic an off-nadir or limb viewing condition, we integrate the IWC profile along different slant paths by adding IWC at each unit

[2] http://wrf-model.org

volume [Fig. 1c]. Therefore in this analysis, without involving interpolation, each path has the same path length, and any differences between the IWCs integrated from different paths are due to cloud internal structural properties. This slantwise integration of IWC, or ice water path (IWP), is the key concept in the current study. If the ice cloud density is randomly distributed in the horizontal direction or homogeneous inside a cloud, the IWP values integrated along the grey (nadir), orange (southward view, or S-view) and green (northward view, or N-view) paths would show no differences. If the cloud ice tilts internally to the left, as shown by the blue ovals in Fig.1c, the IWP along the green path would be the largest among the three paths. Hence, if we define $\Delta IWP = IWP_{|S-view} - IWP_{|N-view}$, **a positive (negative)** ΔIWP **value means that the cloud tilts northward (southward)**. In Fig. 1a, the blue line at 17 km height, which represents ΔIWP integrated between 11 and 17 km with a view-angle of 77°, is negative at the south flank and positive at the north flank of the deep convections down below, which indicates an outward divergent flow. In Fig. 1b, the blue line at 5 km height, corresponding to ΔIWP integrated between 5 and 11 km with the same view-angle, has a positive sign in most places, which translates to a systematic northward tilt of mid-level frontal clouds. These two real cases demonstrate the validity of our method. The same method is applied to WRF simulations to infer cloud tilt structures.

In theory, ΔIWP can be computed from different pairs of slantwise scan-angles. For example, in the case of Fig. 1c, the equivalent scan angle is 77° as the tangent value of 77° equals to the CloudSat grid box length/width ratio (i.e., $tan77° =$1.1 km/0.25 km). The IWC profile is initially interpolated to 250 m vertically (roughly the original vertical resolution), and the slantwise IWP is then calculated by staggering every 1, 2, 3 and 4 grids each time, which translates to a view-angle of 77°, 65°, 56° and 48°, respectively. Meanwhile, cloud count (CC) is also memorized should any positive IWC value appear on the corresponding slantwise path of mass integration. As CC is also different between paired slantwise paths, ΔIWP is technically defined as $\frac{\sum IWP_{|S-view}}{\sum CC_{|S-view}} - \frac{\sum IWP_{|N-view}}{\sum CC_{|N-view}}$ to take such an impact into consideration. Results from the 77° view-angle will be shown in the following section based on the fact that the resulting patterns remain largely robust for all 4 pairs of angle. Since interpolation was not conducted along the slantwise path, neither interpolation-associated spurious signals nor scan angle depen-

dency exists. As the tropical ice clouds usually extend from 5 km to 17 km (Wu et al. (2009)), the cloud structure is therefore divided into two equally thick layers for analysis: 5-11 km and 11-17 km, in order to give them equal weight during the analysis process. The 11 km level also roughly separates the middle and upper troposphere at the tropics. In each layer, the cloud center of mass is assumed to be in the middle of the layer for the location registration (e.g., the location of the black box in Fig. 1c). The parallax issue (Marchand et al. (2007), Wu and Kayava (2013)) is mostly solved by this assumption through large sample integration. Furthermore, since ΔIWP is computed instantaneously for slantwise and nadir views, the local time difference issue which is unavoidable for cross-track scanners is eliminated, although we can only infer the cloud meridional tilt structure here. Same method is likewise applied to the DARDAR product. This paper will focus on presenting the systematic cloud tilt structure in the upper-troposphere (UT) between 11 and 17 km in the tropics. The results in the lower level, which has some limitations, will be shown for completeness.

Finally, Aura Microwave Limb Sounder (MLS) radiance (T_B) data at 640 GHz is used to illustrate the potential impact of our finding on satellite retrievals. The 640 GHz channel has a weighting function peaking at tangent height $\sim$ 12 km, and it is only sensitive to ice cloud. By averaging the 20 saturated radiance measurements at the bottom of each scan, we can treat the averaged radiance as those measured from the slant views by a nadir sounder rather than from a limb column, which help distill the complex cloud information [Wu and Eckermann (2008)]. The MLS 640 GHz forward-looking has an even shallower viewing angle (86°). Therefore, by defining $\Delta T_B = T_{B_{|night}} - T_{B_{|day}}$, we can mimic the slantwise "scan-angle" that is used to compute the CloudSat ΔIWP. However, MLS ΔT_B contains all-sky information from the cloud structure, cloud diurnal variation and other signals in the upper troposphere. Hence, the analysis results using MLS observation have to be interpreted with a lot of caution. Details will be discussed in section 4.

3 Upper-troposphere cloud tilt in the tropics

By differencing the CloudSat IWP in the upper troposphere (11-17 km) along the 77° viewing angles (S-view minus N-view), we found that UT ice cloud mass in the tropics tilted systematically poleward in both hemispheres, as shown in the left panel of Fig. 3 for the December-January-February (DJF) and right panel for the June-July-August (JJA) composites. The time separation roughly characterizes two broad tropical deep convective zones, namely South America, South Africa and Western Pacific during DJF, and west of Central America, West Africa, and Asian Monsoon region including the Maritime Continent during JJA. The maps derived from ascending and descending orbits separately are highly similar to each other (not shown). Given the fact that CloudSats orbit is not strictly perpendicular to the equator (82° angle at the equator), any signal from the zonal direction projected to the orbit track would be opposite sign between the ascending and descending orbits. Therefore, the highly consistent geographic patterns between the day (ascending) and night (descending) imply that the signals should mainly originate from the meridional direction rather than the zonal direction. The relative importance of the mass asymmetry due to the systematic tilt, as measured by $\Delta IWP/IWP$, could easily reach up to 20% near the two flanks of the aforementioned tropical deep convective zones (Fig. 2c and 2d). The sign of the difference is consistent among all four view-angle pairs (not shown), except that the magnitude increases with increasing view angle values, indicating that the UT ice cloud mass is tilted in a very shallow angle with respect to the horizon ($\leq 90° - 77° = 13°$). Yet, these clouds are not completely flat, which should otherwise result in no difference of IWP between paired views. Similar analysis has also been carried out with DARDAR IWC profiles, and the patterns are highly consistent with what were found from CloudSat except that the magnitude of the difference is slightly smaller while the relative importance remains the same order of magnitude (Fig. 4). This is to be expected for IWP as CloudSat alone can detect the majority of cloud ice. The broad consistency between CloudSat and DARDAR analysis results show the robustness of our findings.

From Fig. 3 and Fig. 4 , we see that the patterns are more zonal during JJA than those during DJF, mainly because the continental deep convective centers are located further south during

DJF than the latitude migration of the Inter-tropical Convergence Zones (ITCZ). The upward diverging feature is not only ubiquitous in the tropics, but also present at the north and south flanks of mid-latitude summer active convection regions such as the Southern Pacific Convergence Zone (SPCZ) during DJF, and central United States and the Southern Europe during JJA, where deep convective towers often penetrate upward beyond the 11 km level. Note that the smoothing window is narrower in the top panels of Fig. 3 to highlight these mid-latitude details. The major reason that no signals were found from the rest of mid-latitude area is due to a shallower tropopause height there ($<$ 11 km). Same analyses were performed by truncating the mid-latitude troposphere into 5 - 8 km and 8 - 11 km sectors. Systematic poleward tilt is discovered in the 8 -11 km layer cloud in the winter mid-latitude along storm tracks (not shown). Therefore, we should not interpret you much about the relative importance maps in the mid-latitude as the sample size is very limited above 11 km.

Intuitively, the systematic cloud tilt should be somewhat related to the local or general circulation. In the meridional direction at the tropics, the Hadley Cell dominates the tropospheric circulation, which has the convergence flow at the lower level in the tropics, and divergence flow at the upper level in the subtropics. In reality, Hadley Cell has a complicated longitudinal structure. The cloudy-sky meridional wind derived from Modern-Era Retrospective analysis for Research and Applications (MERRA) analysis datasets is overlaid as arrows in Fig. 3a and 3b to illustrate the divergent upper-level branch of the Hadley Cell circulation in most places over the tropics. Here, the cloudy-sky is defined as MERRA IWC larger than 10 mg/m^3 anywhere between 11 and 17 km in altitude. The divergent flow is generally larger at the peripheries of the active tropical convective regions than that close to the centers, coinciding with the largest cloud asymmetry patterns. This suggests that the systematic UT cloud mass tilt does somewhat follow the general circulation in the meridional direction at the tropics. However, the meridional wind in the Asian monsoon and Maritime Continents region during JJA is predominantly southward, while the UT cloud mass tends to tilt the same way as other regions in the tropics. The dominant southward flow in this area is associated with pan-continent scale anti-cyclonic monsoon circulation, yet the cloud mass tilt is not controlled by this large-scale circulation but still follows the Hadley-cell type of divergence flow pattern. More interestingly, the results

suggest that UT cloud mass tilt does not follow the shape of the tropopause that slopes down away from the equator. The implications will be discussed in the next section. The meridional wind over central US and Southern Europe during JJA is very small and non-divergent, again indicates that the UT cloud tilt does not always follow the general circulation.

Ice cloud tilt in the middle troposphere (5-11 km) still has some ambiguities due to large uncertainties embedded in IWC retrievals below 9 km for heavily precipitating cases. Even if we could exclude those cases, IWC itself cannot reveal the entire cloud mass/shape structure in the lower level as liquid and mixed-phase clouds dominate that level (e.g., the rounded bottom of deep convective clouds of Fig. 1a between $9^{\circ}N$ and $10^{\circ}N$). Preliminary results from CloudSat suggest that 5-11 km ice cloud mass at the tropics tilt the opposite way with that in the UT (i.e., equatorward, part of which will be shown in Fig. 6b), although the cloudy-sky wind in that altitude range is still weakly divergent in the broad picture as suggested by MERRA analysis and Multi-angle Imaging SpectroRadiometer (MISR) mid-level wind datasets (not shown). Meanwhile, mass tilt in this altitude range is barely statistically significant at a 95% confidence level as noted in DARDAR (not shown). Given the fact that the ice mass tilt in the middle troposphere is largely debatable, we will show using the WRF simulations that CloudSat results might be more reasonable.

As seen in Fig. 3d, the UT cloud tilt is relatively more important along the ITCZ cloud bands to the west of Central America and Central Africa, while the situation is more complicated and less important in the Asian monsoon region. Therefore, west of Central America (WCA) with a relatively simple surface condition is an ideal region to conduct a numerical experiment to investigate the underlying causes of the observed tilt.

In the WRF experiments, we randomly selected three days within one month to initialize the simulation (1, 15, 30 August 2009). Each simulation lasted for 2 days. The National Center for Environmental Prediction (NCEP) Global Forecast System (GFS) Final Analyses (FNL) served as the boundary and initial conditions. In a nested configuration, the model has a primary domain (D01) with a 30-km horizontal resolution, a secondary domain (D02) with a 10-km horizontal resolution, and the innermost domain (D03) with a 3.3-km horizontal resolution. Each nested domain is driven along the lateral boundary conditions supplied by the parent domain

with coarse resolution. The domain map is shown in Fig. 5. The vertical resolution is roughly 500 m from the surface up to 50 hPa (the model top). The inner domain boundary is [118°W, 77°W], [2.5°S, 22.5°N]. No damping of vertical motion or gravity wave is specified. As part of the provided microphysical scheme in WRF, the Morrison double moment scheme with forecast for 6 hydrometers in every time step was employed for all runs [Morrison et al. (2009)]. Since the cumulus parameterization has been turned off in D03, this configuration can reasonably capture the cloud vertical structure, despite the fact that clouds smaller than 24 km in horizontal and 4 km in vertical directions ($\sim 8 \times$ grid size) would be significantly under-resolved. Results from D02 with cumulus parameterization served as the sensitivity experiment to test whether realistic convection without subgrid-scale parameterization is the key to reproduce the observed cloud slantwise tilt. The hourly output from D02 and D03 was first interpolated to 250 m vertical and 1.1 km horizontal resolution and then analyzed and averaged together to represent the climatological mean condition.

Overall, D03 simulations show impressive agreement with CloudSat observation in terms of the geographical distributions of the mean IWP and the systematic ice cloud mass tilt in both the middle and upper troposphere. Given the fact that we are comparing 6-day simulations (with a hourly outputs; Fig. 6c and 6d) with 12 months of CloudSat overpass samples in the same region (Fig. 6a and 6b), the D03 simulations are good enough to qualitatively represent the climatological spatial patterns of middle-level converging and upper-level diverging cloud mass tilt. The cloud structural inclination again fits the conceptual picture of flow convergence in the lower level and divergence in the upper level within the rising branch of the Hadley Cell. As the simulated mean IWP shows two centers of enhancement in the upper troposphere, the systematic upward diverging cloud tilt structures occur at the north and south flanks of both centers separately (Fig. 6c). This feature again demonstrates that systematic cloud tilts in the UT always occur at the meridional peripheries of deep convective centers but not within the center.

In the middle troposphere, most ice clouds are convective cumulus. Some of previous case studies suggested that the tilt of convective core within a convective system could experience a life cycle of downwind, upright and upwind with respect to the local wind shear (Weisman and

Rotunno (2004), Lane and Moncrieff (2010)). By far, the climatological characteristic of the vertical orientation of deep convective cumulus has not been well studied nor understood. According to Fig. 6d observed by CloudSat and Fig. 6e simulated by WRF D03 experiment, both of which show generally opposite patterns to the UT ice clouds, we can reach the conclusion that the mid-level ice cloud mass tends to exhibit a "converging" signature on a climatological mean. However, the discrepancy between DARDAR and CloudSat observations in the mid-level is still not explained. Also, the magnitude of ΔIWP is 5-10 times smaller in D03 simulation than that observed by CloudSat. The smaller ΔIWP in D03 may probably be attributed to the coarse model resolutions (3.3 km) that could not explicitly resolve enough details of the cloud structures. On the contrary, simulation results from D02 do not reproduce the observed mean IWP distribution and the mass asymmetries (Fig. 6e and 6f). Hence, we can conclude that the shutdown of cumulus parameterization (thereby, allowing the model to resolve clouds) is the key to successful generation of the systematic cloud mass tilts. In other words, realistic representation of convective processes is fundamental in capturing the cloud inhomogeneity.

UT systematic cloud tilt could introduce a non-trivial error on limb/sub-limb satellite retrievals of ice cloud mass. In this paragraph, we aim to check whether same issue could present for ground instrument as well. To realize such a purpose, slantwise integration paths are now set to start from the ground (technically 3 km to avoid topography) upward and end at an altitude of 19 km, and the cloud location is now registered at the starting point of integration. The entire idea is illustrated in Fig. 7. Note that the southward view still means looking southward, but opposite to the satellite-based view. This ground-based concept should be differentiated from the previous "satellite-based view" shown in Fig. 1c. Here, the focus is to study the impact from the systematic ice cloud tilt on ground instrument measurement, rather than the physics of cloud vertical orientation. With this consideration, 19 km rather than 17 km was chosen as the ending point of mass integration since ice cloud rarely penetrates up beyond 19 km. Fig. 8 gives the IWP difference of ground-based view from four pairs of view-angle versus the nadir-view (Fig. 8a) and ΔIWP between paired views computed from CloudSat data(Fig. 8b). Surprisingly, slantwise IWP is only slightly smaller than the nadir IWP; the largest discrepancy, observed at the most oblique views (equivalent to 76°) is only 4% of the mean IWP across all

latitudes. This is mainly originated from a slightly larger cloud occurring frequency at oblique view angles. Through the total column integration, the south-north difference induced by the systematic cloud tilt is also trivial compared to nadir mean (Fig. 8b). However, if we integrate from 11 km upward to 19 km using the ground-base viewing geometry, the results look almost identical to Fig. 3 (not shown). This is somewhat as expected since it is no fundamental difference from the satellite view shown in Fig. 1c, and parallax effect should only be important to the boundaries of each grid box. As was explained and shown by Fig. 6b and 6d before, mid-troposphere ice cloud tilt presents opposite direction of its counterpart in the UT region. This ground-based view study reveals that their effects can be largely cancelled through the total column integration, and therefore, we can conclude that systematic ice cloud tilt may not induce a potential uncertainty to ground cloud measurements. Consequently, it is not a concern either for satellite nadir or near-nadir measurements that penetrate through the total column of atmosphere.

4 Formation mechanism and importance of systematic UT cloud tilt

CloudSat, DARDAR observations and WRF cloud-resolving simulations all suggest that systematic UT cloud mass tilts tend to occur at the northern and southern peripheries of tropical deep convective regions. The corresponding cloudy-sky meridional wind climatology indicates that the observed/simulated systematic cloud tilt is likely associated with local large-scale divergent wind, which is a part of the Hadley Cell circulation. However, this explanation does not hold at the Asian monsoon region; neither at the summer central United States or Southern Europe, the latitudes of which beyond the reach of the rising branch of the Hadley Cell. More importantly, the largest systematic asymmetries do not occur near the most active convective centers where wind divergence is the largest. Besides, the upward sloping of UT cloud cannot be attributed to the meridional wind only. At 5-11 km, Hadley circulation computed from the reanalysis wind is weakly divergent. Therefore, the possible 5-11 km ice cloud equator ward tilt cannot attributed to the general circulation, either. Our results suggest that the structural characteristics of UT clouds, including anvils and cirrus, are not simply controlled by the large-scale

general circulation. The local in-cloud circulation must be critical.

We propose the climatological adding and cancelling effect as the major cause of the observed cloud tilt pattern. As depicted by the conceptual diagram in Fig. 9, each individual convective cloud or cloud system would form such an upward diverging cloud structure at the upper-level due to mass and momentum continuity. Within the active convection centers such as the ITCZ belt, a myriad of single convection/convective systems would lead to a large cancellation of the tilt effect, and only at the northern-most and southern-most flanks can we identify such a net adding effect of systematic cloud inclination. It is remarkable that the adding effect dominates over the cancelling effect across such a wide latitude range (5 - 10 degrees). This hypothesis may also explain the features occur in the mid-latitude convective centers during summer seasons. The mid-level converging tilt, if true, may be also attributed to this adding and cancelling effect assuming the slantwise orientation of the convective core is determined by lower level wind below 5 km. Further analysis of wind-cloud tilt relationship is required to confirm this hypothesis. Unfortunately, due to the lack and difficulty of in-cloud wind measurements, we cannot test this hypothesis in this paper. It is also of great interest to study details of the in-cloud wind versus tilt angle relationship that is possibly affected by other factors (e.g., CAPE, vertical velocity, different stage of cloud development, etc.).

Clearly, neglecting systematic cloud tilt in satellite retrieval can result in additional biases especially for limb sensors (e.g., Microwave Limb Sounder), nadir sensors at slantwise view-angles (e.g., AIRS, MODIS), and conical sensors (e.g., Clouds and the Earth's Radiant Energy System). For example, Gong and Wu [2011; 2013a] acknowledged the impact on AIRS cloudiness in the zonal direction, where they concluded that up to 50% of AIRS view-angle asymmetry could be attributed to the systematic westward tilted cloud structures in the UT. Aura Microwave Limb Sounder (MLS) day (night) forward-looking view is analogous to CloudSat northward (southward) looking view with a shallower viewing angle ($\sim 86^{\circ}$). Therefore, the cloud ΔT_B between MLS descending and ascending orbits contain mixed information from the cloud structures and cloud diurnal variation. This is a common issue for other cross-track sensors as well. Strikingly, the night and day radiance difference (ΔT_B) from MLS forward scan at 640 GHz (peaking at $\sim$12 km) has a high degree of agreement with the IWP difference

derived from CloudSat observation in terms of geographic locations and magnitudes, as shown in Fig. 10. The highly consistent pattern strongly suggests that systematic cloud tilt contributes to a significant part of MLS ΔT_B signal. Based on our current study, the slantwise ice cloud mass orientation would result in 5 - 20% errors in IWP or IWC retrievals using an off-nadir scan angle. The errors would be systematic at the north and south flanks of the tropical deep convective centers with a latitude width of 5 - 20 degrees. Same order of magnitude of uncertainty would also be present inside the active convective centers when performing individual cloud profile retrieval, despite that the climatological impact is probably trivial due to the cancellation effect from large sampling. One should hence always be cautious of interpreting the ascending-descending difference purely as cloud diurnal variations, or over-correcting all angle-dependent cloud asymmetries as observational biases/artifacts.

The against-tropopause shape and against-mean meridional wind cloud mass tilt has strong implications on the dynamical impact of cloud associated momentum and energy transport. We found from this study that structural characteristics anvils and cirrus tended to be determined by in-cloud circulation rather than the prevailing general mean flow. Moreover, the UT ice cloud mass tilt seems not to be controlled by the low-level wind shear, because it remains the same between CloudSat ascending and descending orbits when the mid-latitude summer convections are at different stages [Weisman and Rotunno (2004)]. Are cloud induced momentum and energy fluxes at the tropopause level particularly strong over the regions where the systematic cloud mass tilt is the most apparent? Cloud-resolving scale of modeling studies (beyond what has been done here initially) are required to answer such kind of questions.

This study also has some implications on CRE evaluation. Studies have shown that CRE in the UT region also affected the cross-tropopause mass transport of atmospheric constituents [Corti et al. (2006), 2006]. Cloud inhomogeneity within satellite footprint has been treated with sophisticated schemes by some satellite observational teams (e.g., CERES) in the calculation of SW CRE, but the LW CRE calculation has not taken the cloud vertical asymmetry so far into consideration [Loeb et al. (2005); Loeb et al. (2007)]. Although thick cloud is opaque at IR band, thin clouds like cirrus are not. IWP difference from observing a slantwise tilted cirrus at off-nadir views is expected to be positively correlated with TB difference at IR channels,

causing an angle-dependent LW CRE estimation. Wu and Liang (2005) claimed that LW CRE was different by 8 - 16% between realistic vertical overlapping (i.e., vertical geometry) and the maximum-random assumption using a month long cloud resolving simulation, which was on the same order of SW CRE uncertainty and in the same range of our estimation. Discrepancies among active and passive satellite sensors on the derived LW CRE may be partly attributed to the tilted cloud structures as well [Li et al. (2011)]. Cloud tilts also affect the precipitation/rain pattern. For example, Wu and Liang (2005) found that the estimates of surface rainfall were greatly improved when they switched the cloud-overlapping scheme from a standard option to a physical-based one.

5 Conclusions

By integrating and differencing CloudSat/DARDAR ice water content (IWC) along a pair of symmetric slant views, we find that tropical upper troposphere (UT, 11 - 17 km) ice cloud mass is ubiquitously tilted. The most prominent tilts occur in the north and south flanks of tropical deep convective centers such as the Asian monsoon region and the Inter-Tropical Convergence Zones (ITCZs). The UT clouds in the tropics generally produce poleward-tilt ice columns, rendering significant view-angle dependent cloud ice differences. The slant-view IWPs can differ by 5 - 20% from opposite scan angles, depending on what view angle is used. Cloud-resolving scale WRF model simulations over the western Central America ITCZ showed good agreement with the CloudSat-observed cloud tilt structures at 11-17 km heights. Moreover, both CloudSat and WRF simulations suggest a mid-level (5 - 11 km) cloud mass converging tilt as well, while the total column integration of the opposite tilted structures largely cancel the effects of each other.

These cloud tilt characteristics are consistent with the convective outflow from tropical deep convection as a result of mass conservation. The constructively adding and cancelling effect of a large ensemble of tilted cloud ice mass, driven by in-cloud circulation, can explain the geographic distribution of systematic cloud mass tilt. However, due to lack of accurate in-cloud wind measurements, the proposed hypothesis has not been verified and remains to be tested in

the future study.

This study for the first time presents a global characterization of cloud tilt structures in the middle and upper troposphere. The observed IWP differences in the paired slant-views have important implications for remote sensing and modeling of global cloud systems, including satellite retrieval of cloud properties, atmospheric momentum and energy budget, CRE calculation, and modulation of the hydrological cycle. The study raises more questions than answers, notably the wind-tilt angle relationship, and potential impacts on energy, momentum and hydrological cycles. More importantly, as GCMs continue to improve their resolution (e.g., NICAM, [Satoh et al. (2008)]), vertically tilt cloud structures will become explicitly resolved. The modeled cloud 3D inhomogeneity will need and subject to verification or scrutiny against the observations as shown in this study.

Acknowledgements. This work is performed at the NASA Goddard Space Flight Center with support from the NASA NNH10ZDA001N-ESDRERR (Earth System Data Records Uncertainty Analysis) project. V. L. was supported by the National Science Foundation (NSF) under grants AGS-1116123 and AGS-MRI-0958616 and the Coastal Carolina University Kerns Palmetto Professorship endowment. The CloudSat data processed and stored at Colorado State University is appreciated. All data from this study is available upon request by sending email to the corresponding author.

References

Austin, R. T., A. J. Heymsfield, and G. L. Stephens: Retrievals of ice cloud microphysical parameters using the CloudSat millimeter-wave radar and temperature, J. Geophys. Res., 114(D00A23), dpi:10.1029/2009JD010049, 2009.

Cahalan, Robert F., William Ridgway, Warren J. Wiscombe, Thomas L. Bell, Jack B. Snider: The Albedo of Fractal Stratocumulus Clouds, J. Atmos. Sci., 51, 24342455, 1994.

Corti, T., B. P. Luo, Q. Fu, H. Vomel, and T. Peter: The impact of cirrus clouds on tropical troposphere to stratosphere transport, Atmos. Chem. Phys., 6, 25392547, 2006.

Delanoe, J., and R. J. Hogan: Combined CloudSat-CALIPSO-MODIS retrievals of the properties of ice clouds, J. Geophys. Res., 115, D00H29, doi:10.1029/2009JD012346, 2010.

Delanoe, J., A. Protat, O. Jourdan, J. Pelon, M. Papazzoni, R. Dupuy, J.?F. Gayet, and C. Jouan: Comparison of airborne in-situ, airborne radar-lidar, and spaceborne radar-lidar retrievals of polar ice cloud properties sampled during the POLARCAT Campaign, J. Atmos. Oceanic Technol., 30, 5773, doi:10.1175/JTECH-D-11-00200.1, 2013.

Eliasson, S., G. Holl, S. A. Buehler, T. Kuhn, M. Stengel, F. Iturbide-Sanchez, and M. Johnston: Systematic and random errors between collocated satellite ice water path observations, J. Geophys. Res., 118, 1-14, 2013.

Fu. Q., B. Carlin, G. Mace: Cirrus horizontal inhomogeneity and OLR bias, Geophysical Research Letters, 27:20, 3341-3344, 2000.

Gong, J., and D. L. Wu: View-angle dependent AIRS cloud radiances: Implications for tropical anvil structures, Geophys. Res. Lett., doi:10.1029/2011GL047910, 2011.

Gong, J., and D. L. Wu: View-angle dependence of AIRS cloudiness and radiance variance: Analysis and interpretation, J. Geophys. Res., doi:10.1002/jgrd.50120, 2013.

Gong, J., and D. L. Wu: CloudSat-constrained cloud ice water path and cloud top height retrievals from MHS 157 and 183 GHz radiances, Atmos. Meas. Tech., 7, 1873-1890, doi:10.5194/amt-7-1873-2014, 2014.

Hong, G., G. Heygster, J. Miao, and K. Kunzi: Potential to estimate the canting angle of tilted structures in clouds from microwave radiances around 183 GHz, 2(1), 40-44, 2005.

Huang, D., C. Zhao, M. Dunn, X. Dong, G. G. Mace, M. P. Jensen, S. Xie and Y. Liu: An intercomparison of radar-based liquid cloud microphysics retrievals and implications for model evaluation studies, Atmos. Meas. Tech., 5, 14091424, 2012, doi:10.5194/amt-5-1409-2012, 2012.

Lane, T. P., and M. W. Moncrieff: Characterization of momentum transport associ- ated with organized

moist convection and gravity waves, J. Atmos. Sci., 67, 32083225, 2010.

Li, J. M., Y. H. Yi, P. Minnis, J. P. Huang, H. R. Yan, Y. J. Ma, W. C. Wang, J. K. Ayers: Radiative effect differences between multi-layered and single-layer clouds derived from CERES, CALIPSO, and CloudSat data. Journal of Quantitative Spectroscopy and Radiative Transfer, 112:2, 361-375, 2011.

Liang, X.-Z., and X. Wu: Evaluation of a GCM subgrid cloud-radiation interaction parameterization using cloud-resolving model simulations, Geophys. Res. Lett., 32, doi: 10.1029/2004GL022301.

Li, J., H. W. Barker: Accounting for unresolved clouds in a 1D infrared radiative transfer model. part I: solution for radiative transfer, including cloud scattering and overlap, J. Atmos. Sci., 59, 3302-3320, 2002.

Loeb, N. G., S. Kato, K. Loukachine, and N. Manalo-Smith: Angular distribution models for top-of-atmosphere radiative flux estimation from the Clouds and the Earth's Radiant Energy System instrument on the Terra satellite. Part I: Methodology, J. Atm. Ocn. Technol., 22, 338-351, 2005.

Loeb, N. G., S. Kato, K. Loukachine, N. Manalo-Smith, and D. R. Doelling: Angular distribution models for top-of-atmosphere radiative flux estimation from the Clouds and the Earths Radiant Energy System instrument on the Terra satellite. Part II: Validation, J. Atm. Ocn. Technol., 24, 564-584, 2007.

Marchand, R. T., T. P. Ackerman, and C. Moroney: An assessment of Multiangle Imaging Spectroradiometer (MISR) stereo-derived cloud top heights and cloud top winds using ground-based radar, lidar, and microwave radiometers, J. Geophys. Res., 112, D06204, doi:10.1029/2006JD007091, 2007.

Ming, M., and Z. Zhang: On the influence of cloud fraction diurnal cycle and sub-grid cloud optical thickness variability on all-sky direct aerosol radiative forcing, J. Quant. Spec. and Rad. Trans., 142, 25-36, doi:10.1016/j.jqsrt.2014.03.014, 2014.

H. Morrison, G. Thompson, and V. Tatarskii: Impact of Cloud Microphysics on the Development of Trailing Stratiform Precipitation in a Simulated Squall Line: Comparison of One- and Two-Moment Schemes. Mon. Wea. Rev., 137, 9911007. doi: http://dx.doi.org/10.1175/2008MWR2556.1, 2009.

Naud, C. M., A. D. Del Genio, M. Bauer, W. Kovari: Cloud vertical distributions across warm and cold fronts in CloudSat-CALIPSO data and a general circulation model, J. Clim., 23, 3397- 3415, 2010.

Oreopoulos, L., Lee, D., Sud, Y. C., and Suarez, M. J.: Radiative impacts of cloud heterogeneity and overlap in an atmospheric General Circulation Model, Atmos. Chem. Phys., 12, 9097-9111, doi:10.5194/acp-12-9097-2012, 2012.

Protat, A., D. Bouniol, J. Dalanoe, E. OConnor, P. T. May, A. Plana-Fattori, and A. Hasson: Assessment of CloudSat reflectivity measurements and ice cloud properties using ground-based and airborne cloud radar observations, J. Atmos. Ocn. Technol., 26, 1717-1741, 2009.

Satoh, M., T. Matsuno, H. Tomita, H. Miura, T. Nasuno, S. Iga: Nonhydrostatic icosahedral atmospheric model (NICAM) for global cloud resolving simulations, J. Computational Phys., 227(7), 3486-3514, doi: 10.1016/j.jcp.2007.02.006, 2008.

Weisman, M.L., and R. Rotunno: A theory for strong long-lived squall lines re- visted, J. Atmos. Sci., 61, 361-382, 2004.

Dong L. Wu and Stephen D. Eckermann: Global Gravity Wave Variances from Aura MLS: Characteristics and Interpretation. J. Atmos. Sci., 65, 36953718. doi: http://dx.doi.org/10.1175/2008JAS2489.1, 2008.

Wu, D. L., R.T. Austin, M. Deng, S.L. Durden, A.J. Heymsfield, J.H. Jiang, A. Lambert, J.-L. Li, N.J. Livesey, G.M. McFarquhar, J.V. Pittman, G.L. Stephens, S. Tanelli, D.G. Vane, and D.E. Waliser: Comparisons of global cloud ice from MLS, CloudSat, and other correlative data sets, J. Geophys. Res, 114, D00A24, 2009.

Wu, D. L. and M. J. Kayava: CGMS working paper global wind measurements from earth orbit atmospheric motion vectors and development of Doppler Lidar Systems, CGMS-41 NASA-WP-05, 2013.

Wu, X. Q., X.-Z. Liang: Radiative effects of cloud horizontal inhomogeneity and vertical overlap identified from a month-long Cloud-Resolving Model simulation, J. Atmos. Sci., 62, 41054112, 2005.

Yuan T. and L. Oreopoulos: On the global character of overlap between low and high clouds, Geophys Res Lett., doi:10.1002/grl.50871, 2013.

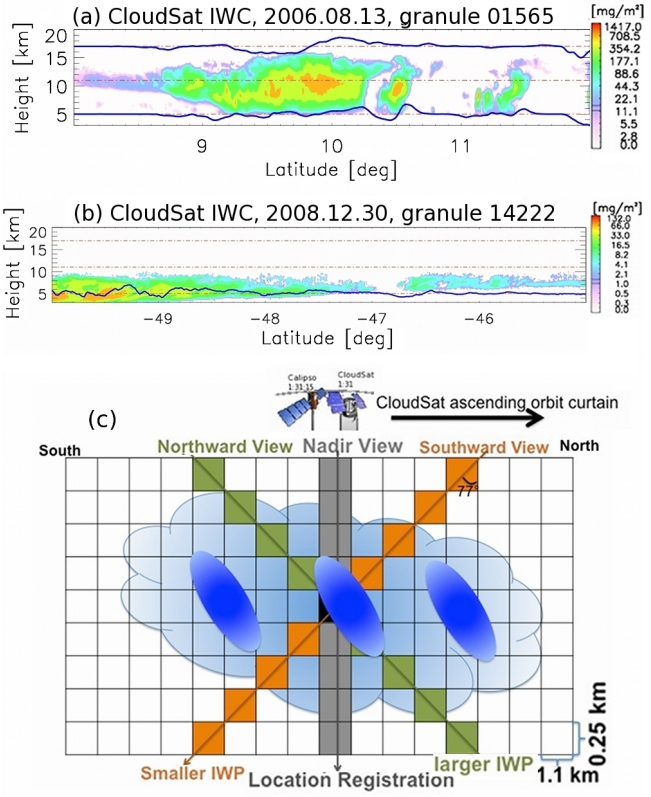

Fig. 1. (a) and (b) show examples of ice water content (IWC) curtain from CloudSat 2B-CWC-RO product (V008). The curtains are divided into two sectors as indicated by the black dash-dot lines. Color scale is linear with largest (smallest) value in orange (white). The blue curves whose zero values are centered around the 5 km and 17 km vertical level illustrate the ice water path differences (ΔIWP) derived from the algorithm demonstrated in the diagram (c) for layer 5 - 11 km and 11 - 17 km. See text for details of (c) and the sign convention of the blue curves. The ratio is approximately 4:1 between horizontal and vertical scales for all panels, therefore, 77° looks like 45° in (c) because of the squeeze of the horizontal scale.

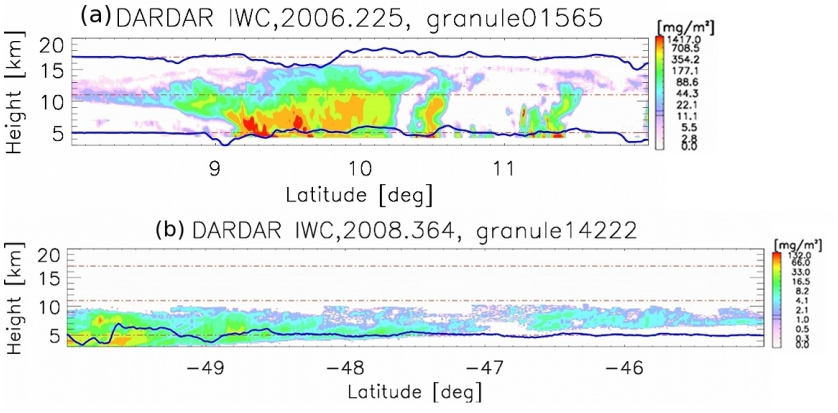

Fig. 2. IWC curtains (color shades) from DARDAR-Cloud v2.1.1 retrieval products for the two cases shown in Fig. 1. Color scale is linear, and is ranged between the maximum DARDAR IWC value within the curtain (red) and 0 (white). One can only find subtle differences in the IWC and ΔIWC (blue solid lines) values, but cloud is in general more ubiquitous in the DARDAR product. For example, DARDAR ice cloud product reveals a thin cirrus layer above the anvil clouds in the tropical deep convection case that is not detected by CloudSat.

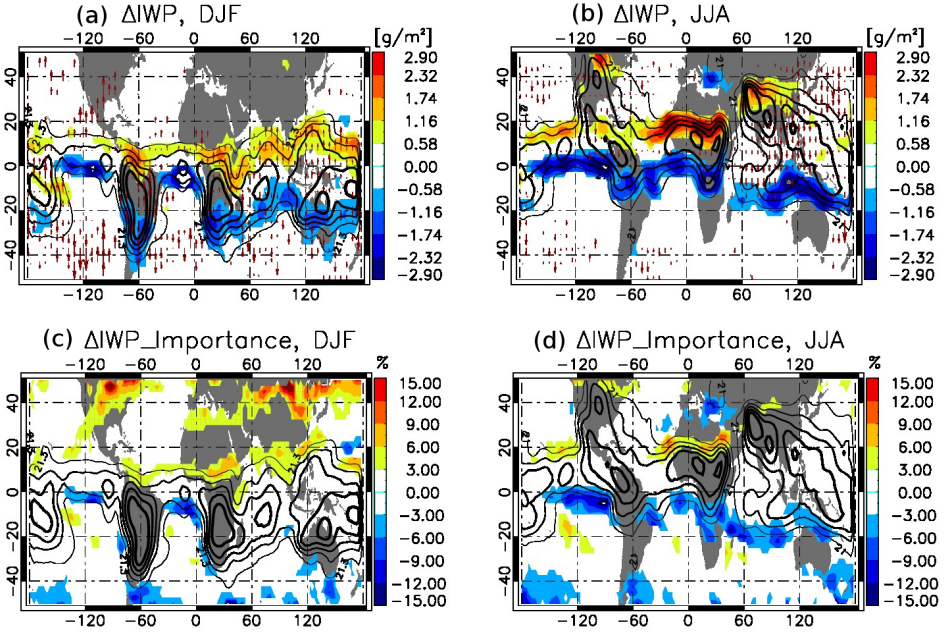

Fig. 3. ΔIWP (color shades; unit is g/m^2) between the south-view and the north-view with view-angle of 77° for December-January-February (a) and June-July-August (b) averaged during 2007-2010 between 11 and 17 km. Results are based on CloudSat IWC dataset within $\pm 50°$ latitude range. The corresponding percentage difference of IWP (i.e., $\Delta IWP/IWP$, color shades; unit is %) is shown in (c) for DJF and (d) for JJA. The mean IWP within this altitude range is contoured in black with the contour interval equal to the minimum value shown on the contour line. MERRA cloudy-sky meridional wind climatology during the same period is shown in arrow in (a) and (b) with wind speed linearly proportional to the arrow length. The longest arrow corresponds to 16 m/s in (a) and 9.15 m/s in (b). Data in the top panels are smoothed by a 2×2 smoothing window.

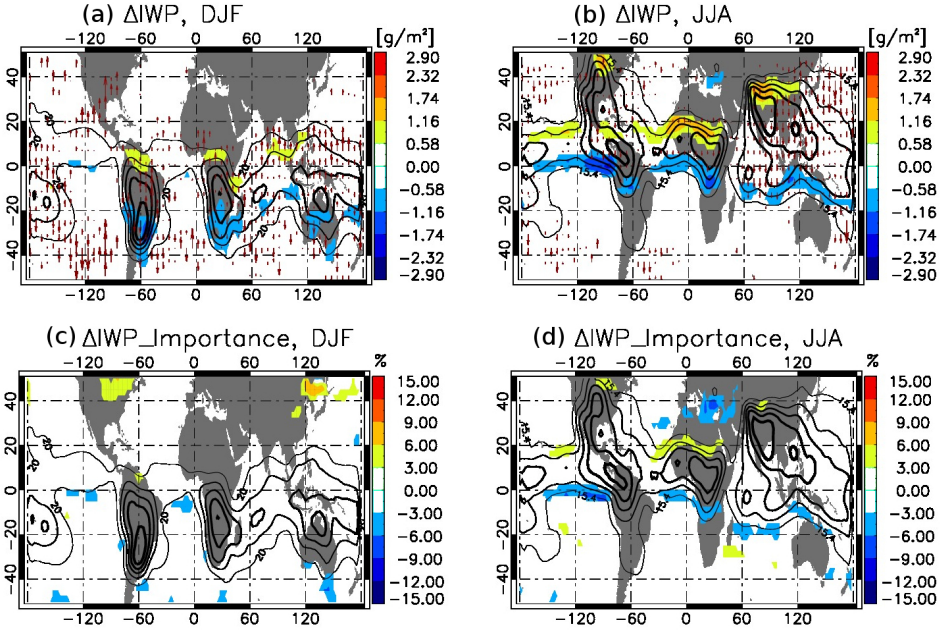

Fig. 4. Same with Fig. 3, except for using DARDAR v2.1.1 IWC product within the same altitude range.

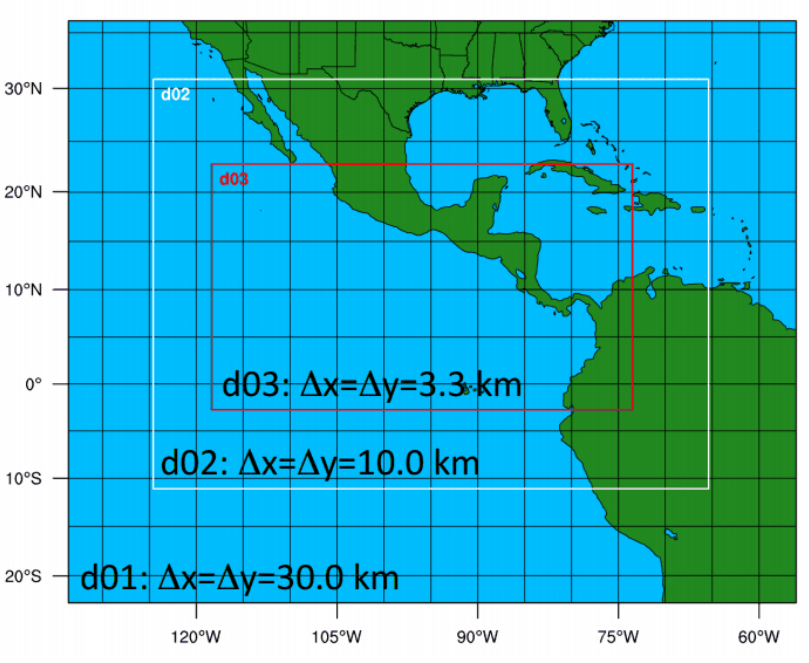

Fig. 5. The domain map of WRF nested simulations.

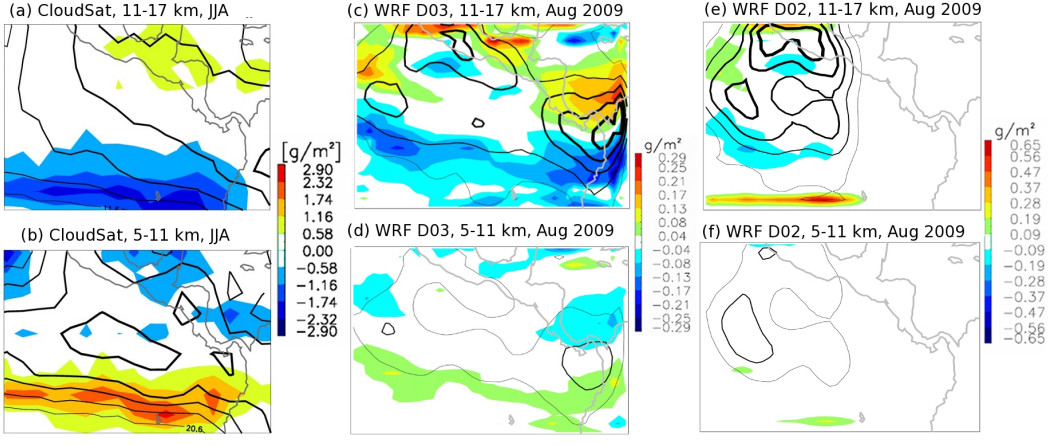

Fig. 6. Climatological ΔIWP (color shades) derived from CloudSat at 77° view angle during JJA, 2007-2010 for ice clouds within 11-17 km (a) and 5-11 km (b), and the same variable derived from WRF D03 (c & d) and D02 (e & f) domains at 77° view angle. The black contours mark the mean IWP integrated along the nadir view within the corresponding altitude range. Note that the magnitude of ΔIWP from WRF run is much smaller than that from the CloudSat observation.

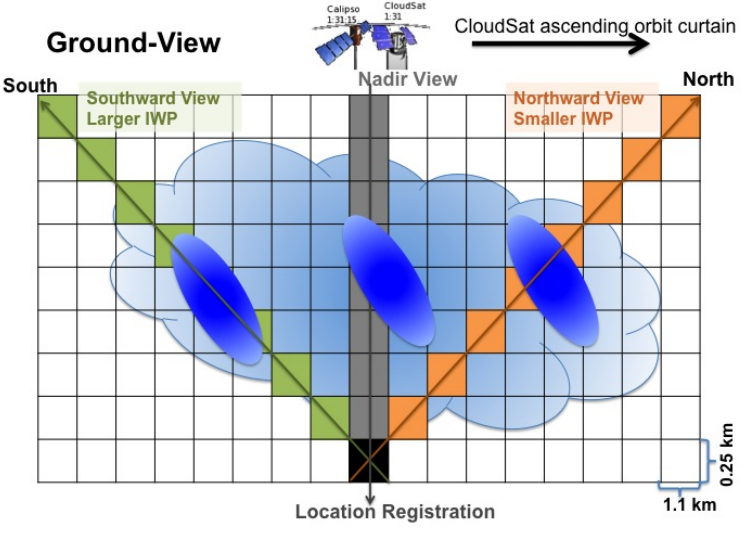

Fig. 7. A diagram showing the computation geometry of the ground-view.

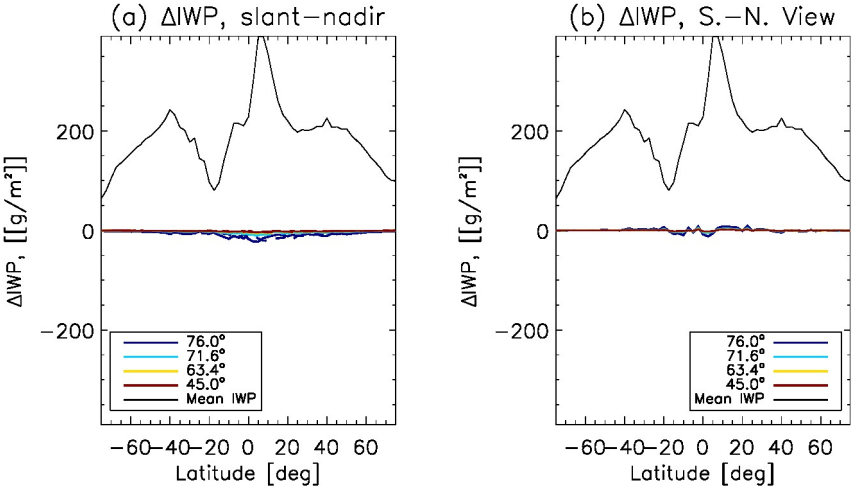

Fig. 8. Ground-based view of (a) latitudinal distribution of JJA ΔIWP between nadir and southward-looking view (solid lines), nadir and northward-looking views (dashed lines with the same color of solid lines). (b) latitudinal distribution of JJA ΔIWP between southward-looking and northward-looking views (solid color lines) integrated from 5 km to 19 km. The black solid lines are the mean IWP at nadir. Refer to Fig. 7 for viewing geometry).

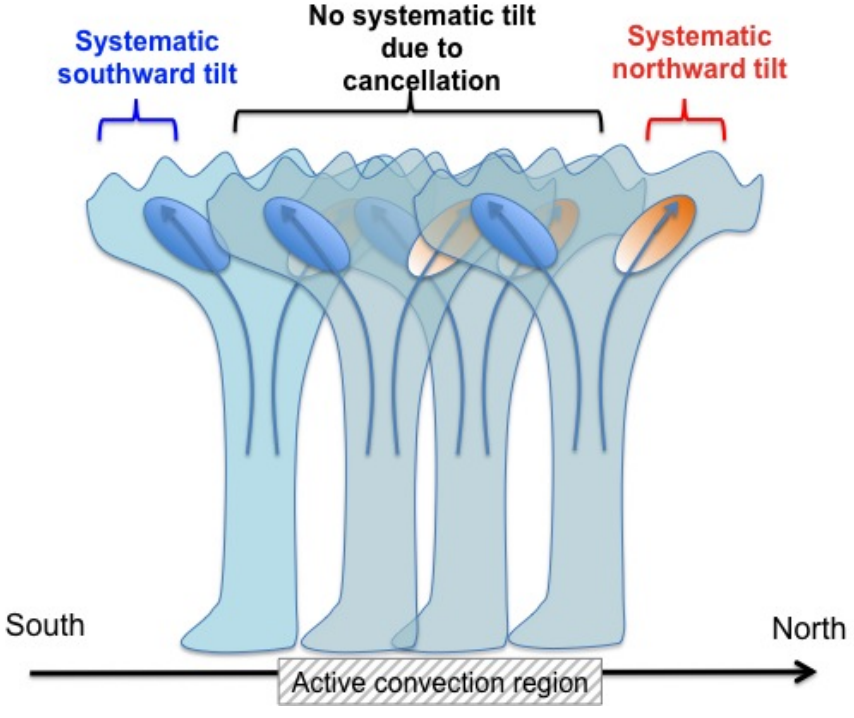

Fig. 9. Schematic diagram showing the explanation of systematic poleward UT cloud tilts at the north and south peripheries of active tropical convection regions.

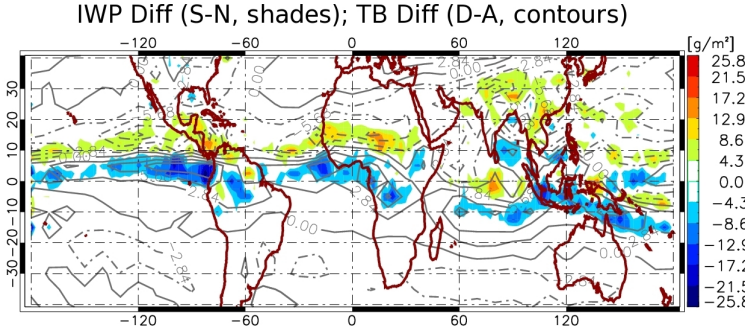

Fig. 10. CloudSat ΔIWP (color shades) and Aura MLS 640 GHz ΔTB (descending minus ascending orbits to mimic CloudSat viewing geometry, contours, dashed is negative, while solid is positive) for JJA, 2007-2010. The maps are interpolated to $2^\circ \times 2^\circ$ grid box, and the correlation coefficient is -0.68. Note that MLS has a shallower viewing angle, and it has a cloud diurnal cycle embedded in the signal.